Acta Materialia 215 (2021) 117036

Contents lists available at ScienceDirect

Acta Materialia

journal homepage: www.elsevier.com/locate/actamat

Full length article

Preparation of zinc oxide/poly-ether-ether-ketone (PEEK) composites via the cold sintering process

Mingming Si[a], Jianyu Hao[b], Enda Zhao[b], Xuetong Zhao[c], Jing Guo[a,*], Hong Wang[a,b,d], Clive A. Randall[e]

[a] State Key Laboratory for Mechanical Behavior of Materials & School of Materials Science and Engineering, Xi'an Jiaotong University, Xi'an 710049, China
[b] School of Electronic and Information Engineering, Xi'an Jiaotong University, Xi'an 710049, China
[c] State Key Laboratory of Power Transmission Equipment & System Security and New Technology, Chongqing University, Shapingba District, Chongqing 400044, PR China
[d] Department of Materials Science and Engineering & Shenzhen Engineering Research Center for Novel Electronic Information Materials and Devices, Southern University of Science and Technology, Shenzhen, China
[e] Materials Research Institute and Department of Materials Science & Engineering, The Pennsylvania State University, University Park, PA 16802 United States

ARTICLE INFO

Article history:
Received 2 February 2021
Revised 26 May 2021
Accepted 27 May 2021
Available online 2 June 2021

Keywords:
Cold sintering process
Ceramic matrix composites
Zinc oxide
Polymers
Electro-ceramics

ABSTRACT

Appropriate preparation routes allow designing and improving the performances of ceramic-based functional composites. In this work, two powder-preparation methods enabled by the cold sintering process are utilized to fabricate unique ZnO-based varistor composites. The thermoplastic polymer, poly-ether-ether-ketone (PEEK), has been successfully integrated with ZnO to form dense ZnO-PEEK composites. With a dissolution method, PEEK particles can be homogeneously dissolved by the mixed solution of tetrahydrofuran and toluene and then form nanoscale thin grain boundaries after cold sintering process. In the direct mixing method, large PEEK particles are observed in the cold sintered samples. A Finite Element Method (FEM) analysis indicates that von-mises stresses concentrate at the grain boundaries of ZnO and at the interfaces of ZnO and PEEK, and these can be increased with the increase of PEEK particle sizes. The electrical properties have been improved with the addition of PEEK, and the cold sintered 95ZnO-5PEEK shows a high breakdown electric field (0.1 mA/mm^2) of 3070 V/mm, and a nonlinear coefficient of 5. In addition, the conduction mechanism of the composites has been investigated using impedance spectroscopy. Overall, our work provides a strategy for the development of high-performance ceramic-polymer composites via cold sintering process.

1. Introduction

The poly-ether-ether-ketone (PEEK) is a kind of thermoplastic polymer with excellent comprehensive high temperature properties. It has a long-range order structure with the main chain composed of a ketone bond and two ether bonds. As a semi-crystalline polymer material, its melting point is over 300 °C and the softening point is about 168 °C [1–3]. Due to the outstanding physical and chemical properties including excellent dielectric and mechanical properties, high temperature resistance and chemical corrosion resistance, PEEK can be used as electrical insulating materials and structural materials at high temperatures [4–5]. PEEK polymer has a large number of applications in various fields, including the aerospace, medical devices, electronics, automobile industries, etc.

Zinc oxide (ZnO) is a semiconducting material with a wideband gap of ~3.37 eV [6–9]. It has a large exciton binding energy, high transparency, and excellent luminous properties at room temperature. As a semiconductor oxide, it is widely used in liquid crystal displays, thin film transistors, light emitting diodes, varistors, etc. [10,11]. ZnO based varistors are key materials for circuit protectors in electronic devices and overvoltage arresters in power systems. The main electrical parameters of ZnO based varistors include breakdown electric field (E_b) and nonlinear coefficient (α), Typically, a variety of metal oxides such as Bi_2O_3, Co_2O_3, MnO_2, Sb_2O_3, SiO_2, etc. [12–20] are sintered into ZnO to form the Schottky barriers at the grain boundaries and improve the overall electrical performances under conventional sintering conditions with temperatures from ~1000 to 1200 °C.

* Corresponding author.
E-mail address: jingguo19@xjtu.edu.cn (J. Guo).

https://doi.org/10.1016/j.actamat.2021.117036
1359-6454/

Traditionally, one of the main routes to prepare ceramic-polymer composites is to disperse ceramic materials in the polymer matrix to improve the structural or electrical properties of the polymers [9,21]. As for the ceramic-based composites, ceramic powders are usually sintered first to form ceramic skeletons, followed by the infiltration of polymers [22,23]. The differences of sintering temperatures between ceramics and polymers make it difficult to fabricate ceramic-based composites without damaging the polymers in a single step.

The melting temperature, T_m of ZnO is 1975 °C [9] and the sintering temperature, T_s, is usually >1000 °C within the expected conventional thermal sintering-range $0.5<T_s/T_m<0.95$, which is incompatible with co-processing polymeric materials. Cold sintering process (CSP) has recently emerged as a low temperature (≤300 °C) sintering technique, with $T_s/T_m<0.2$, potentially offering a manufacturing path with lower energy costs and fast densification increasing process throughput [24–26]. The dissolution-precipitation process is activated with an important selection of a transient chemical phase, that is assisted by an applied pressure and moderate temperature [27]. A large number of ceramic materials in a variety of laboratory scale prototypes have been developed with CSP [26,28,29] or CSP assisted sintering methods [30–32]. Due to the low sintering temperatures, researchers recently have demonstrated the feasibility of integrating polymers into ceramics via CSP, such as Li_2MoO_4-PTFE (Polytetra fluoroethyllene), V_2O_5-PEDOT: PSS (Poly (3,4-ethylenedioxythiophene)-poly (strene sulfonate)), ZnO-PTFE, SiO_2-PTFE, ZnO–$Ca_3Co_4O_9$-PTFE, and ZnO-PDMS (Polydimethylsiloxane) composites [33–35]. ZnO-PTFE, and $BaTiO_3$-PTFE [36] can be cold sintered into high densities with excellent electrical properties. With the modification of grain growth, new properties are introduced [35]. Herisson de Beauvoir et al. show that ZnO-PTFE composites have an anisotropic grain growth after cold sintering, which in turn affects the physical properties in-plane [37]. Dey and Bradt report that (1-x)ZnO-xPDMS composites ($0.00\leq x\leq 0.05$) can be sintered to above 90% of the theoretical density by cold sintering process at 250 °C under a pressure of 320 MPa for 60 min [38].

As for the reported cases on cold sintering, the polymers are typically dispersed in the ceramics by direct mixing, and thus, polymers with small particle sizes are usually required to assist the cold sintering process and improve the properties of the resulted composites. In this work, another mixing route named dissolution method is introduced, where the polymers are dissolved in an organic solvent first and then mixed with ceramic powders. The effects of particle sizes of polymers on the sintering and properties have been studied using Finite Element Method (FEM). Moreover, PEEK is a thermoplastic polymer with a high melting point and excellent physical and chemical properties, and there is no work on cold sintered ceramic-based composites with addition of PEEK up to date. Therefore, it is of interest to integrate PEEK with ZnO by cold sintering process to tailor the interfacial structures and electrical properties.

In this study, PEEK was added into ZnO using two different routes (direct mixing and dissolution method) and then cold sintered to form ZnO-PEEK composite varistors. The relative densities, microstructures, and electrical properties were studied in detail. The mechanism was investigated using FEM with the thermal-mechanical coupling simulation. The results indicate that high performance composites can be obtained using cold sintering process with a high breakdown electric field (0.1 mA/mm^2) of 3070 V/mm, and a nonlinear coefficient of 5.

2. Experiments

The ZnO powder with a particle size of 270–330 nm (99.9%) was obtained from Forsman Scientific (Beijing) Co., Ltd. The PEEK powder with an average particle size of 10 μm (99%) was obtained from Jilin Joinature Polymer Co.,Ltd. Acetic acid, toluene and tetrahydrofuran (99%) were obtained from Sinopharm Chemical Reagent Co.,Ltd.

Table 1
Compositions of ZnO-PEEK powders.

Samples	ZnO (Wt.%)	PEEK (Wt.%)
ZP0	100	0
ZP1	99.75	0.25
ZP'1	99.75	0.25
ZP'2	97.00	3.00
ZP'3	95.00	5.00
ZP'4	93.00	7.00
ZP'5	90.00	10.00
ZP'6	80.00	20.00

2.1. Synthesis of ZnO-PEEK powders

According to the component ratios in **Table 1**, ZnO and PEEK powders were mixed using two different methods to form ZnO-PEEK composite powders. ZnO, PEEK and ZnO-PEEK were abbreviated as Z, P and ZP (or ZP'), respectively. As shown in **Fig. 1**, the first method was to dissolve the PEEK powders firstly, and then to disperse the ZnO powders in the solution. The other one was to mix ZnO powders with PEEK powders straightly by magnetic stirring. **Table 1** lists the weight percentages of all the compositions, among which ZP0, ZP1, and ZP'1-ZP'6 stand for pure ZnO, ZnO-PEEK using the dissolution method (The first mixing route), and ZnO-PEEK using the direct mixing method (The second mixing route). More compositions can be found in the Supporting Information (**Table S1**). The detailed processes are shown as follows.

The first method of preparing ZnO-PEEK powders is shown in **Fig. 1a**. Firstly, 100 mL tetrahydrofuran (THF) and 110 mL toluene were mixed and magnetically stirred for 40 min with a speed of 400 revs/min. Then, the PEEK powders were put into the mixed solution at a ratio of 0.40 g/100 mL, and magnetically stirred at 40 °C for 1 h. Afterwards, the temperature was set to 71 °C and the stirring process was continued for 3 h. Then, the ZnO powders were poured into the mixed solution and stirred for 1.5 h at 71 °C. After that, the mixed solution was poured into a ball mill jar and mechanically ground for 4 h with a rotating speed of 1000 revs/min. Finally, the mixed solution was dried at 90 °C for 12 h. The ZnO-PEEK powders were sieved through an 800-mesh screen.

The second method of preparing ZnO-PEEK powders is shown in **Fig. 1b**. ZnO and PEEK powders were mixed and ball milled for 4 h in ethanol using a planetary ball mill tank with a rotating speed of 450 revs/min. Then, the mixed solution was placed into an oven and baked at 90 °C for 12 h. Finally, it was filtered through an 800-mesh screen.

2.2. Cold sintering process

1.0 g ZnO-PEEK powders and 0.13 g acetic acid aqueous solution (1.5 mol/L) were mixed using an agate mortar. After homogeneous mixing, the wetted powders were poured into a steal die. In the case of ZPi or ZP'j ($i = 1$; $j = 1, 2, \ldots, 6$) samples, the die was pressed under a uniaxial pressure of 300 MPa and heated to 330 °C at a heating rate of 5 °C/min with a holding time of 120 min, after which the sample was naturally cooled down to room temperature. In the case of pure ZnO (ZP0), the wetted powders were pressed with a load of 218 MPa and cold sintered at 220 °C for 70 min.

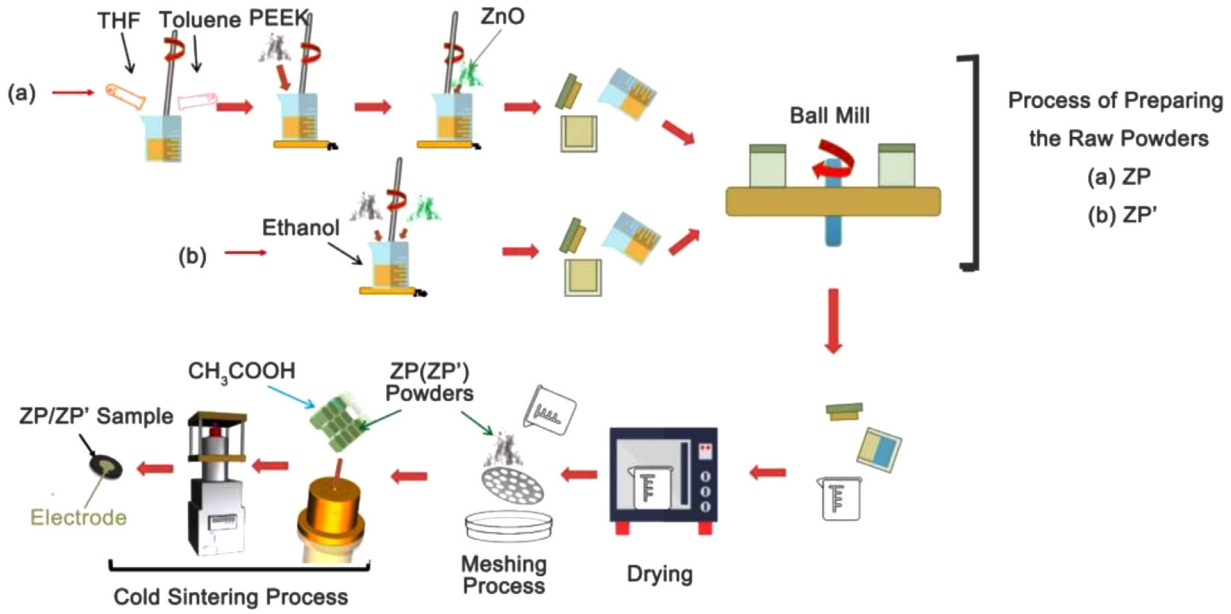

Fig. 1. Schematic illustrating the mixing routes for ZnO-PEEK powders and the cold sintering process of the composites. **(a)** Dissolution method (ZP). **(b)** Direct mixing method (ZP').

2.3. Characterizations

The final densities of cold sintered samples were determined by Archimedes's method (XS204 Analytical Balance) and geometric method. Structures were characterized by X-Ray diffraction (XRD) on cold-sintered pellets with Cu Kα radiation (PANalytical Empyrean). The 2θ angles range from 7° to 70° with a scanning step of 0.026°. Microstructures were observed by SEM (LS 10, CARL ZEISS EVO MA10) and FE-TEM (JEOL JEM-F200 (HR)). The SEM images were obtained from both surfaces and fractured surfaces of cold sintered samples. Prior to the measurement of SEM on surfaces, the samples were polished using sandpapers with 800 mesh, 1200 mesh and 1um diamond polishing agent. The TEM specimens were prepared using the focused ion beam (FIB, FEI Helios NanoLab 600i). Before electrical measurements, the samples were polished with sandpapers and Au electrodes were sputtered on both sides of the samples using a sputter coater. The Current-Voltage was measured by a high-voltage test system (PolyK, USA) and a temperature chamber (Delta 9023, Delta Design, Poway, CA). The impedance spectroscopies and dielectric properties were measured in the frequency range of 100mHz-8 MHz (Electrochemical workstation, Zennium-Pro 43,139, ZAHNER, Germany) and 100Hz-10 MHz (Keysight E4990A), respectively.

3. Results and discussion

Fig. 2**a** shows the densities and relative densities of cold sintered ZnO-PEEK composites (More details are shown in **Table S2, Supporting information**). It is seen that the relative densities of ZP0, ZP1 and ZP'1 are 99.96%, 98.80% and 98.74%, respectively, indicating that highly dense ZnO-PEEK composites can be obtained by the cold sintering process. It is also seen that with the increase of PEEK amount, the densities and relative densities of the composites show a downward trend (more details can be found in the microstructural analysis). As shown in Fig. 2**b**, there are no obvious impurities detected in the XRD patterns and all the sharp peaks can be indexed to wurtzite ZnO with a PDF No. 800,074. The XRD peaks representing PEEK are difficult to be observed with the content of PEEK less than 7wt%. When the content of PEEK reaches over 7wt%, a weak and broad peak belonging to PEEK can be detected. The XRD result indicates that ZnO does not react with PEEK and ZnO-PEEK composites can be formed under the cold sintering conditions.

Fig. 3**a–c** and **Fig. S1 (Supporting Information)** present the microstructures of ZnO-PEEK raw powders. In the case of the dissolution method (ZP1), PEEK particles with 10 μm are dissolved homogeneously in the THF and toluene solution, so that large PEEK particles are not observed in ZP1 samples, as seen in Fig. 3**b**. In the case of the direct mixing method (ZP1'), there are obvious large particles (PEEK) detected besides the small zinc oxide particles, as shown in Fig. 3**c** and **Fig. S1**. With the content of PEEK increases, PEEK particles are more and more unevenly dispersed. The agglomeration has been occurred in some areas in powder ZP'5 and ZP'6. Fig. 3**d–f** and **Fig. S2** (**Supporting Information**) show the cross-sectional SEM images of the cold sintered samples with different amounts of PEEK. The SEM images of polished surfaces of ZP0, ZP1 and ZP'1 can be found in **Fig. S3 (Supporting Information).** Both ZP1 and ZP1' have compact microstructures with few pores between the grains, which are similar to the pure ZnO. With increasing the amount of PEEK, more pores can be found, as shown in **Fig. S2**, which is in a good agreement with the density data. The PEEK particles are located between ZnO grains, preventing the mass transportation of ZnO, which leads to a decreasing tendency of the relative densities.

Fig. 3**g–i** and **Fig. S4** (**Supporting Information**) are EDS results of all the ZnO-PEEK composites after cold sintering process. The mixed solution of THF and toluene can dissolve the PEEK particles within a certain limit so that small PEEK particles can be homogeneously distributed along the ZnO grains in sample ZP1. However, for the samples with the direct mixing method (ZP'1-ZP'6), PEEK shows larger particle sizes with a lamellar shape. More proofs for the distribution of PEEK in ZP1 and ZP'1 can be found in **Fig. S5** (**Supporting Information**).

Fig. 4 shows the TEM micrographs of cold sintered ZnO-PEEK composites. From the overview in Fig. 4**a**, it can be clearly seen that there are two phases in sample ZP1, and PEEK is homogeneously dispersed in ZnO, which is in consistent with the SEM analysis. Fig. 4**b,c** are enlarged images from Fig. 4**a** to show the details of the interfaces between ZnO and PEEK. As an amorphous phase, PEEK is located in the grain boundaries with a thickness of

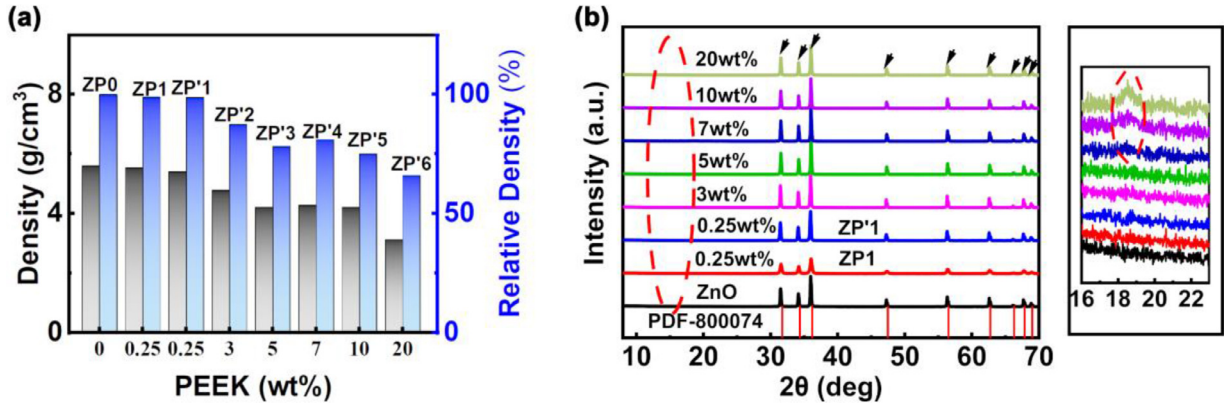

Fig. 2. **(a)** The densities and relative densities of the ZnO-PEEK composites with the amount of PEEK ranging from 0 to 20wt%, **(b)** XRD data of the cold sintered ZnO-PEEK composites.

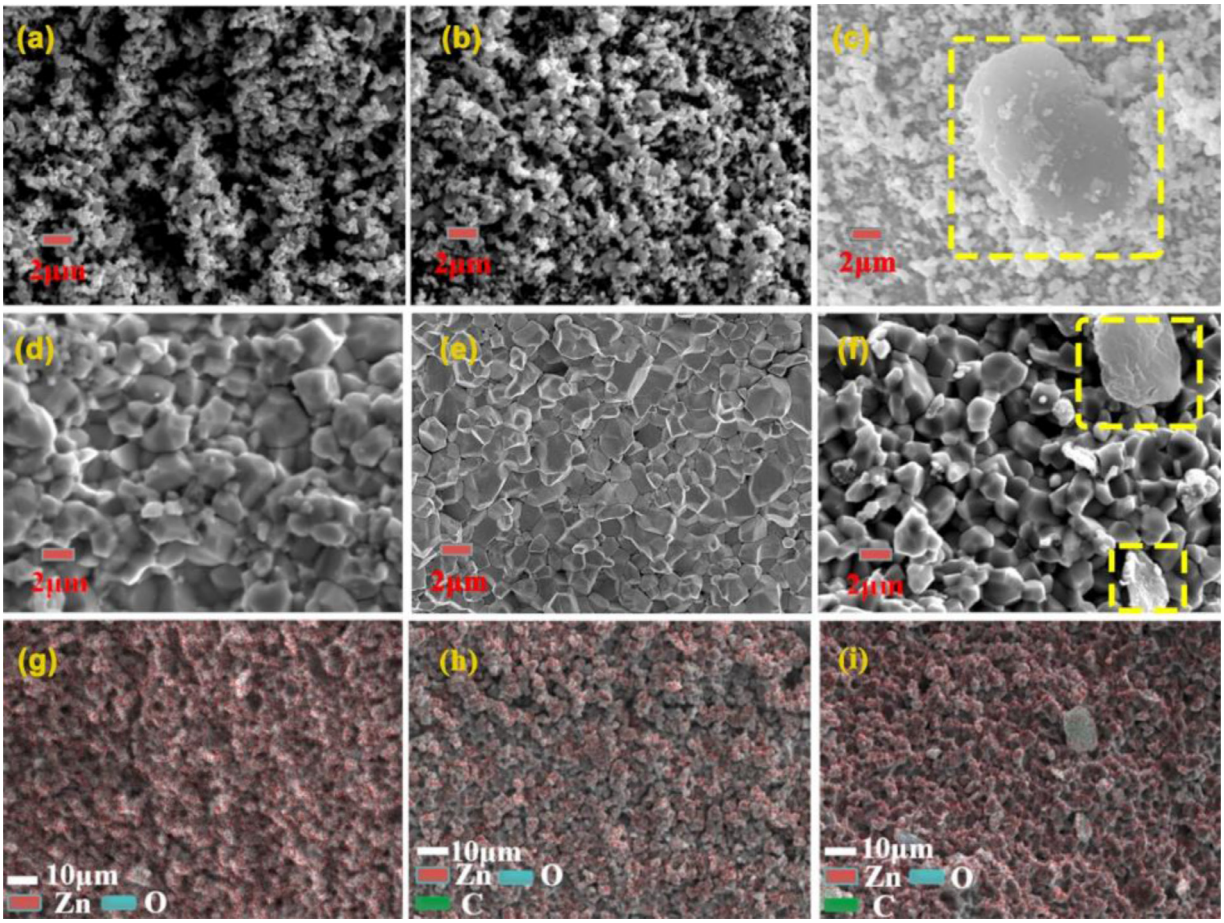

Fig. 3. SEM micrographs of ZnO-PEEK powders and cold sintered samples, and the related EDS mapping results. SEM images of Powder ZP0 **(a)**, ZP1 **(b)**, and ZP'1 **(c)**. SEM images of the cross sections of cold sintered ZP0 **(d)**, ZP1 **(e)**, and ZP'1 **(f)**. EDS mapping results of cold sintered ZP0 **(g)**, ZP1 (**h**), and ZP'1 **(i)**.

tens to hundreds of nanometers. This phenomenon further demonstrates that PEEK is dissolved by the THF and toluene solutions and transported to the ZnO grain boundaries during cold sintering process.

In order to study the effects of the PEEK particle sizes on the structures and properties, a 2D thermal-mechanical coupling simulation has been performed using an ideal micro-model with FEM, as shown in **Fig. S6 (Supporting Information)**. ZnO and PEEK are assumed to be ideal hexagonal particles with a side length of 1.0 mm, and circular particles with diameters of 0.1 mm and 0.2 mm (or elliptical particles), respectively. All the particles are flexible and the parameters are based on the literatures. The constraints of the simulation model are shown in **Fig. S6a**. To simplify the analysis, the mass transportation through the liquid phase is ignored in the simulation calculation.

Fig. 5 depicts the calculation results of the von-mises stresses for different models (the result is magnified by 80 times so that the difference can be clearly seen). It is seen that the stresses concentrate at the grain boundaries of ZnO and interfaces of ZnO and PEEK. With the increase of the PEEK particle sizes, the von-mises stresses around the PEEK particles show an increase trend, which is similar to the results of von-mises strains (**Fig. S6,** S**upporting**

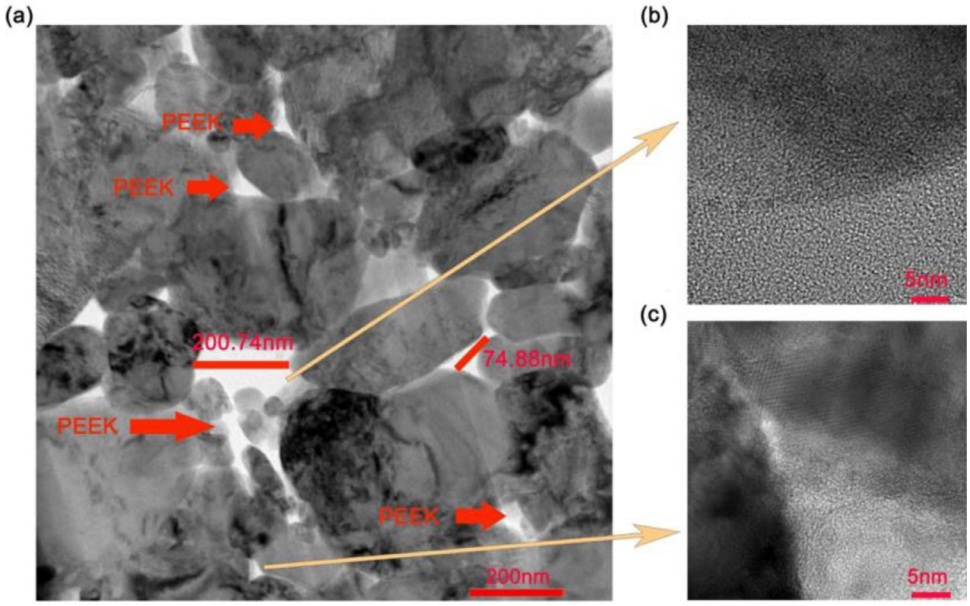

Fig. 4. TEM images of cold sintered sample ZP1. (**a**) Overview, (**b**) The interface between ZnO and PEEK characterized by a high-resolution transmission electron microscopy, (**c**) ZnO-PEEK-ZnO boundaries.

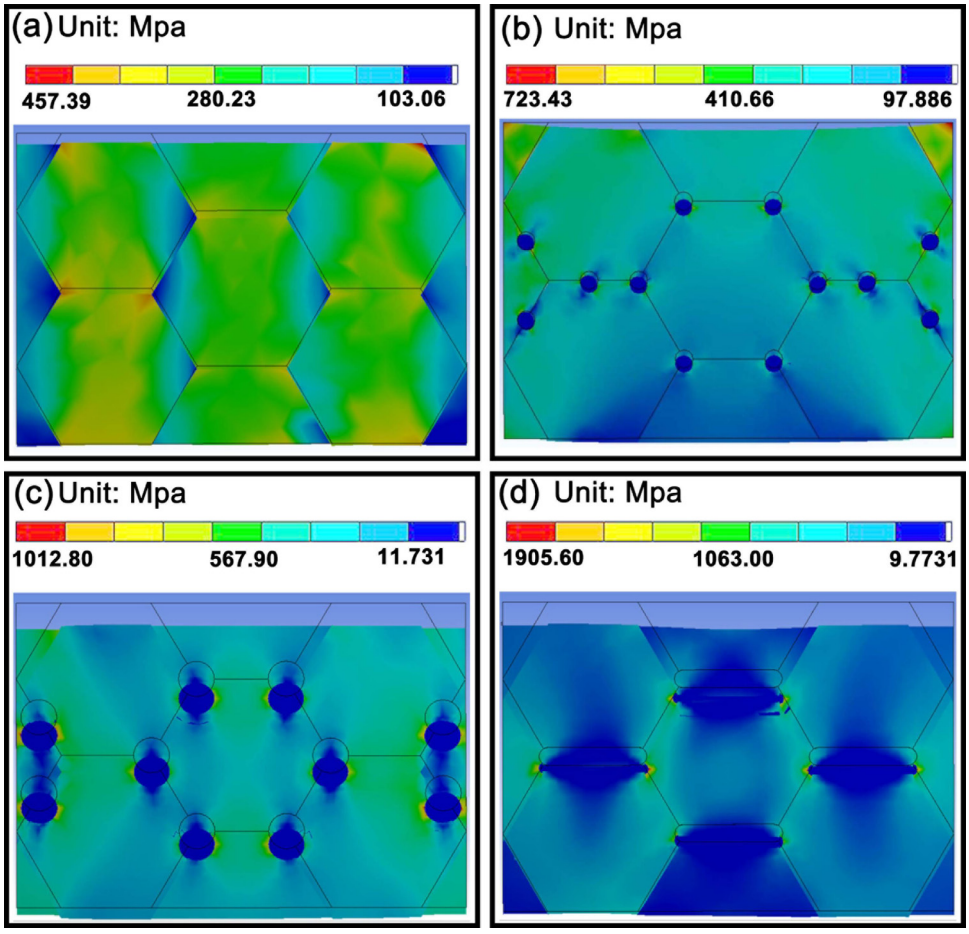

Fig. 5. Calculation results of Finite Element Method. Von-mises stresses of the pure ZnO model (**a**), ZnO with circular particles with a diameter of 0.1 mm (**b**) and 0.2 mm (**c**), and ZnO with oval particles (**d**).

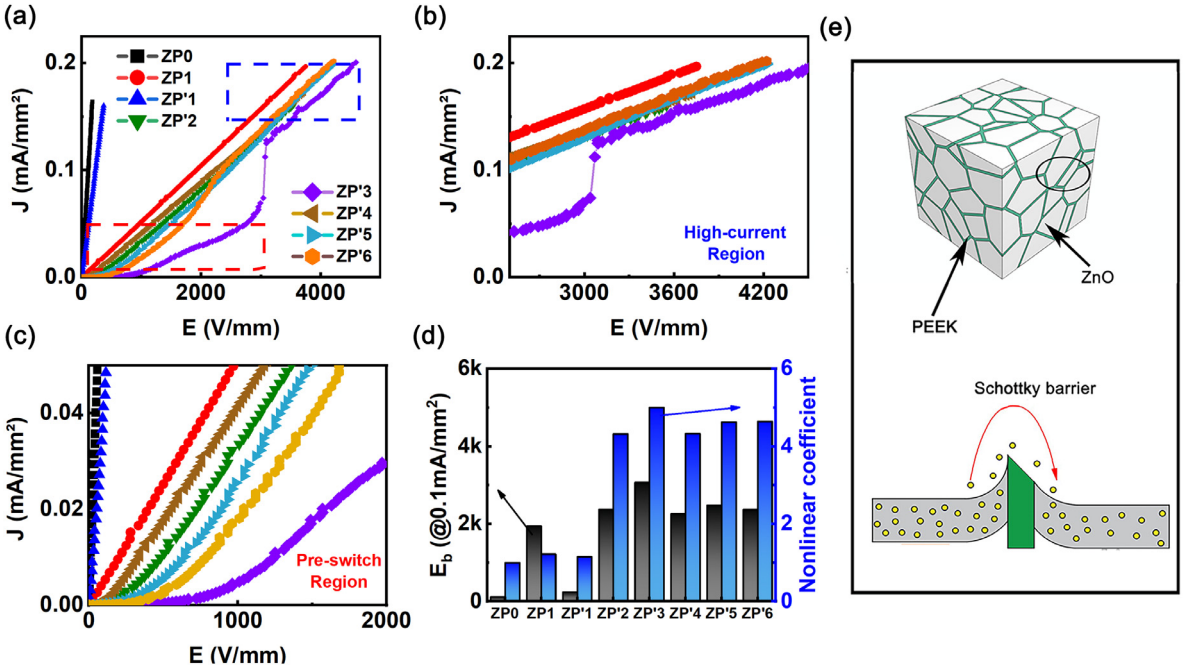

Fig. 6. **(a)** Current density - electric field (*J-E*) curves of the cold sintering samples at room temperature, **(b)** The high current regions of the *J-E* curves, **(c)** The pre-switch regions of the *J-E* curves, **(d)** The breakdown electric field at 0.1 mA/mm^2 and the nonlinear coefficient of the ZnO-PEEK composites, **(e)** A schematic of the barrier at the grain boundaries.

I**nformation**). The stresses of the interfaces can be enhanced from several hundred MPa to over GPa with PEEK particle sizes increasing. It is also seen that when the shape of PEEK particles is changed from circle to oval, both the stresses and strains of the contact areas are increased. The excessive stresses during cold sintering process may lead to more defects at the interfaces, which affects the electrical properties of ZnO-PEEK composites.

The breakdown electric field (E_b) and non-linear coefficient (α) are important indicators for examining the electrical performances of the varistors. In this work, the generic nonlinear Current-Voltage characteristics are obtained using the formula as follow [38,39],

$$\alpha = \log I / \log U \tag{1}$$

Where α is the nonlinear coefficient; I and U are the current and voltage, respectively. The breakdown regions of some varistors appear in advance or lag, and α can also be calculated by fitting the actual *I-V* curves of the samples. If α=1 and α>1, the samples would be regarded as an ohmic resistor and varistor, respectively. The higher nonlinear coefficient, the better performance the varistors will have.

Fig. 6a–c depict the *E-J* curves of the cold sintered ZnO-PEEK composites with different content of PEEK. There are three main regions in a typical *E-J* curve of ZnO based varistors, including pre-switch region, breakdown region and high-current region [36] (**Fig. S7, Supporting Information**). **Fig. 6b,c** show the details of the high-current region and pre-switch region respectively. The calculated nonlinear coefficient and breakdown electric field (0.1 mA/mm^2) are summarized in **Fig. 6d**. It is seen that ZnO shows an E_b of 114.9 V/mm, while all the cold sintered ZnO-PEEK composites have much higher breakdown electric fields and the maximum E_b is obtained in sample ZP'3 with 3070 V/mm, almost 27 times higher than that of pure ZnO. This phenomenon indicates that the addition of PEEK can dramatically improve the breakdown electric fields of ZnO ceramics. It is also seen that the breakdown electric field of ZP1 (1693.6 V/mm) is much higher than that of ZP1' (239.2 V/mm), which may result from that PEEK is more homogenous dispersed in ZnO matrix using the dissolution method and the composite shows fewer defects after cold sintering process (ZP1). The improvement of breakdown electric field via dissolution method also occurs in other compositions, as known in **Fig. S8** (**Supporting Information**).

Comparing the samples ZP'1-ZP'6, it is found that the breakdown electric field shows an increase trend first, and then decreases with increasing the amount of PEEK. It is well known that PEEK is an excellent insulating material with a high breakdown electric field. Therefore, it is reasonable that the breakdown electric field can be enhanced with the addition of PEEK. However, if the amount of PEEK is too high, there will be obvious agglomeration for PEEK particles after cold sintering process, as discussed in the above SEM analysis. The agglomeration is unfavorable for the densification of ceramics, and thus the ZnO-PEEK composite shows a lower density with a high PEEK amount. The lower density and agglomeration of PEEK particles together with the defects lead to the decrease of the breakdown electric field for the amount of PEEK higher than 5wt%.

Based on the microstructural analysis, it is found that PEEK is located at the grain boundaries of ZnO after cold sintering process. The interface of ZnO and PEEK forms a Schottky barrier, which makes ZnO-PEEK composites exhibit nonlinear electrical characteristics [40–44]. **Fig. 6e** shows a schematic diagram of the interfacial barrier of cold sintered ZnO-PEEK composites. With the increase of PEEK content, the nonlinear coefficient shows a trend of increasing first and then decreasing, that is similar to the changes of the breakdown electric field. Sample ZP'3 (5wt% PEEK) has the largest nonlinear coefficient of 5.

Fig. 7a,b and **Fig. S9** (**Supporting Information**) present the dielectric properties of cold sintered samples. Compared with ZnO, PEEK has a smaller dielectric constant, and thus, the dielectric constant of ZnO-PEEK composite is smaller than that of ZnO, as shown in **Fig. 7a** and **Fig. S9a**. Meanwhile, the losses show a similar decrease trend with the addition of PEEK, as seen in **Fig. 7b** and **Fig. S9b**. Impedance spectroscopy is usually used to study the conduction mechanisms of varistors or heterogeneous systems. The contribution of different areas to the conductivity of varistors can be

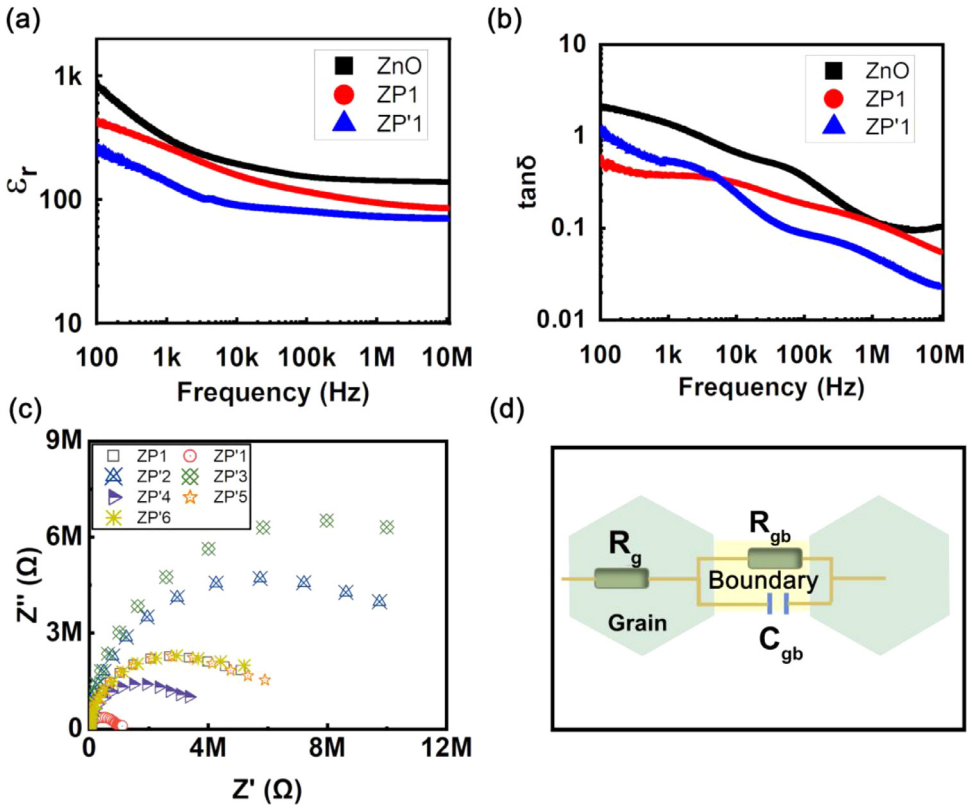

Fig. 7. Dielectric properties and impedance spectra of cold sintered ZnO-PEEK composites. **(a)** Relative dielectric constant, **(b)** Losses, **(c)** Impedance spectra, and **(d)** Equivalent circuit model.

obtained using an equivalent circuit with electronic components [45–47]. The existence of the PEEK phase in the grain boundaries will lead to the formation of Schottky barrier and the difference in characteristics between the grains and the grain boundaries. ZnO grains can be equivalent to the resistance (R), while the grain boundaries can be equivalent to parallel resistance-capacitance (RC) elements. **Fig. 7c,d** show the Nyquist diagram and equivalent circuit of ZnO-PEEK samples with different PEEK contents in the frequency range from 100 mHz to 8 MHz. According to the Nyquist curve, the grain resistance R_g and grain boundary resistance R_{gb} can be obtained using the equivalent circuit model. The calculated R_g and R_{gb} are listed in **Table S3** (**Supporting Information**). It is seen that PEEK can significantly affect the grain boundary resistance. With the increase of the PEEK content, R_{gb} shows a trend of increase first and then decrease. With 5wt% PEEK addition, the ZnO-PEEK composite shows the largest R_{gb}. Similar with the analysis of the I-V characteristics, the changes of the grain boundary resistance may result from the comprehensive factors such as densities, agglomeration of PEEK particles, and the defects.

4. Conclusions

In this work, a new type of ZnO-polymer composites is introduced. The thermoplastic polymer, PEEK, has been first integrated into ZnO via cold sintering process, and dense ZnO-PEEK composites can be obtained by CSP with a dilute acetic acid (1.5 mol/L) at a low temperature of 330 °C. With the addition of 0.25wt% PEEK, the composite shows the highest relative density of over 98%. In the case of the dissolution method, PEEK can be homogeneously dissolved by the mixed solution of tetrahydrofuran and toluene and form small particles in the cold sintered samples. In the case of the direct mixing method, most of the PEEK particles have a similar size to the raw powders after cold sintering process. The FEM analysis reveals that the von-mises stresses concentrate at the grain boundaries of ZnO and interfaces of ZnO and PEEK. The stresses of the interfaces can be enhanced from several hundred MPa to over GPa with PEEK particle sizes increasing, and the excessive stresses may lead to more defects at the interfaces. The I-V characteristics show that ZnO-PEEK composites are varistors, and the largest nonlinear coefficient of 5 can be obtained in the samples with 5wt% PEEK. One of the advantages of ZnO-PEEK composites is that the breakdown electric field can be dramatically improved and the largest E_b is 3070 V/mm (5wt% PEEK), almost 27 times higher than that of ZnO. In addition, due to more homogeneous distribution, ZP1 (dissolution method) shows a higher breakdown electric field than ZP'1 (direct mixing method). The impedance spectra have been fitted using the RC equivalent circuit and the grain boundary resistance shows a trend of increase first and then decrease with the increase of PEEK amount, which is similar with the changes of nonlinear coefficient and breakdown electric field. Comprehensive factors such as densities, agglomeration of PEEK particles, and defects are considered to be the reasons for the changes of electrical properties. In summary, this study provides two routes to prepare functional ZnO-PEEK composites, which may inspire the further study for the cold sintered ceramic-polymer composites.

Declaration of Competing Interest

The authors declare that they have no known competing financial interests or personal relationships that could have appeared to influence the work reported in this paper.

Acknowledgments

The work was supported by the National Natural Science Foundation of China (Grant No. 51902245 and 51877016) and Natural Science Foundation of Shaanxi Province China (No. 2020JQ-044). We would like to thank Ren, Z.J., Chen, Y.N., Li, J., and Li, C. (the Instrument Analysis centre of Xi'an Jiaotong University) for the SEM and TEM measurements. We also thank Lu, L. (the School of Microelectronics and State Key Laboratory for Mechanical Behaviour of Materials, Xi'an Jiaotong University) for the TEM sample preparation using FIB.

Supplementary materials

Supplementary material associated with this article can be found, in the online version, at doi:10.1016/j.actamat.2021.117036.

References

[1] R.C. Batra, A. Pydah, Impact analysis of PEEK/ceramic/gelatin composite for finding behind the armor trauma, Compos. Struct. 237 (2020) 111863.
[2] Y. Zheng, X. Yang, M. Yuan, J. Luo, Synthesis and gas transport properties of novel poly(ether ether ketone)s containing fluorene group, High Perform. Polym. 31 (2019) 1173–1182.
[3] Y. Liu, S. Huang, J. Tan, Z. Wang, Z. Jiang, H. Zhang, PEEK/diatomite composites by *in situ* polymerization: synthesis, characterization and fundamental properties, J. Appl. Polym. Sci. 136 (2019) 46983.
[4] L. Karthikeyan, D. Mathew, T.M. Robert, Poly(ether ether ketone)-bischromenes: synthesis, characterization, and influence on thermal, mechanical, and thermo mechanical properties of epoxy resin, Polym. Adv. Technol. 30 (2019) 1061–1071.
[5] D.J. Kim, B.-.N. Lee, S.Y. Nam, Synthesis and characterization of PEEK containing imidazole for anion exchange membrane fuel cell, Int. J. Hydrog. Energy 42 (2017) 23759–23767.
[6] P. Mao, J. Wang, L. He, L. Zhang, A. Annadi, F. Kang, Q. Sun, Z. Wang, H. Gong, Excellent capacitor-varistor properties in lead-free $CaCu_3Ti_4O_{12}$-$SrTiO_3$ system with a wrinkle structure via interface engineering, ACS Appl. Mater. Interface 12 (2020) 48781–48793.
[7] G.R. Dillip, A.N. Banerjee, S.W. Joo, Template-based synthesis of hollow nanotubular ZnO structures and nonlinear electrical properties under field-induced trap-assisted tunneling, J. Phys. Chem. C 124 (2020) 28371–28386.
[8] S.Y. Chung, I.D. Kim, S.J. Kang, Strong nonlinear current-voltage behaviour in perovskite-derivative calcium copper titanate, Nat. Mater. 3 (2004) 774–778.
[9] J.J. Shea, Metal oxide varistors: from microstructure to macro-characteristics, in: IEEE Electr. Insul. Mag., 36, 2019, p. 3.
[10] S.M. Léna, M.L. Kahn, C. Estournes, D. Tremouilles, M. Bafleur, P. Renaud, B. Chaudret, Size effect on properties of varistors made from zinc oxide nanoparticles through low temperature spark plasma sintering, Adv. Funct. Mater. 19 (2009) 1775–1783.
[11] Y. Wang, Z. Peng, Q. Wang, X.L. Fu, Highly nonlinear varistors from oxygen-deficient zinc oxide thin films by hot-dipping in Bi_2O_3: influence of temperature, Appl. Surf. Sci. 390 (2016) 92–99.
[12] S. Cherumannil Karumuthil, K. Singh, U. Valiyaneerilakkal, J. Akhtar, S. Varghese, Fabrication of poly (vinylidene fluoride-trifluoroethylene)-zinc oxide based piezoelectric pressure sensor, Sens. Actuators A 303 (2020) 111677.
[13] X. Cheng, Z. Lu, X. Liu, W. Yi, Z. Chen, X. Wang, Improvement of surge current performances of ZnO varistor ceramics via C_3N_4-doping, J. Eur. Ceram. Soc. 40 (2020) 2390–2395.
[14] X. Yang, G. Hu, G. Gao, X. Chen, J. Sun, B. Wan, Q. Zhang, S. Qin, W. Zhang, C. Pan, Q. Sun, Z.L. Wang, Coupled ion-gel channel-width gating and piezotronic interface gating in ZnO nanowire devices, Adv. Funct. Mater. 29 (2019) 1807837.
[15] S. Roy, T.K. Roy, D. Das, Grain growth kinetics of Er_2O_3 Doped ZnO-V_2O_5 based varistor ceramics, Ceram. Int. 45 (2019) 24835–24850.
[16] J.M. Carlsson, H.S. Domingos, P.D. Bristowe, B. Hellsing, An interfacial complex in ZnO and its influence on charge transport, Phys. Rev. Lett. 91 (2003) 165506.
[17] F. Fu, D. Yang, H. Wang, Y. Qian, F. Yuan, J. Zhong, X. Qiu, Three-dimensional porous framework lignin-derived carbon/ZnO composite fabricated by a facile electrostatic self-assembly showing good stability for high-performance supercapacitors, ACS Sustain. Chem. Eng. 7 (2019) 16419–16427.
[18] S. Dursun, K. Tsuji, S.H. Bang, A. Ndayishimiye, C.A. Randall, A route towards fabrication of functional ceramic/polymer nanocomposite devices using the cold sintering process, ACS Appl. Electron. Mater. 2 (2020) 1917–1924.
[19] W. Cao, X. Xie, Y. Wang, M. Chen, Y. Qiao, P. Wang, Y. Zhang, J. Liu, Effect of Pr_6O_{11} doping on the microstructure and electrical properties of ZnO varistors, Ceram. Int. 45 (2019) 24777–24783.
[20] D. Xu, K. Song, Y. Li, L. Jiao, S. Zhong, J. Ma, L. Bao, L. Zhang, J. Song, Sc_2O_3 Doped Bi_2O_3-ZnO thin films varistor prepared by sol-gel method, J. Alloys Compd. 746 (2018) 314–319.
[21] M. Arbatti, X.B. Shan, Z.Y. Cheng, Ceramic-polymer composites with high dielectric constant, Adv. Mater. 19 (2007) 1369–1372.
[22] C.W. Nan, Y. Shen, J. Ma, Physical properties of composites near percolation, Annu. Rev. Mater. Sci. 40 (2010) 131–151.
[23] S.Q. Yuan, F. Shen, C.K. Chua, K. Zhou, Polymeric composites for powder-based additive manufacturing: materials and applications, Prog. Polym. Sci. 91 (2019) 141–168.
[24] J. Guo, R. Floyd, S. Lowum, J.P. Maria, T. Herisson de Beauvoir, J.H. Seo, C.A. Randall, Cold sintering: progress, challenges, and future opportunities, Annu. Rev. Mater. Res. 49 (2019) 275–295.
[25] J. Guo, X. Zhao, T. Herisson De Beauvoir, J.-.H. Seo, S.S. Berbano, A.L. Baker, C. Azina, C.A. Randall, Recent progress in applications of the cold sintering process for ceramic-polymer composites, Adv. Funct. Mater. 28 (2018) 1801724.
[26] J. Guo, H. Guo, A.L. Baker, M.T. Lanagan, E.R. Kupp, G.L. Messing, C.A. Randall, Cold sintering: a paradigm shift for processing and integration of ceramics, Annu. Rev. Mater. Res. 55 (2016) 11457–11461.
[27] F. Bouville, A.R. Studart, Geologically-inspired strong bulk ceramics made with water at room temperature, Nat. Commun. 8 (2017) 14655.
[28] S.S. Faouri, A. Mostaed, J.S. Dean, D. Wang, D.C. Sinclair, S. Zhang, W.G. Whittow, Y. Vardaxoglou, I.M. Reaney, High quality factor cold sintered Li_2MoO_4-$BaFe_{12}O_{19}$ composites for microwave applications, Acta Mater. 166 (2019) 202–207.
[29] M. Nelo, T. Siponkoski, H. Khri, K. Kordás, H. Jantunen, Upside - down composites: fabricating piezoceramics at room temperature, J. Eur. Ceram. Soc. 39 (2019) 3301–3306.
[30] J. Gonzalez-Julian, K. Neuhaus, M. Bernemann, D. Silva, J. Pereira, A. Laptev, Unveiling the mechanisms of cold sintering of ZnO at 250 °C by varying applied stress and characterizing grain boundaries by Kelvin probe force microscopy, Acta Mater. 144 (2018) 116–128.
[31] M. Kermani, M. Biesuz, J. Dong, D.H. Jiu, S. Grasso, Flash cold sintering: combining water and electricity, J. Eur. Ceram. Soc. 40 (2020) 6266–6271.
[32] J. Nie, Y. Zhang, J.M. Chan, R. Huang, J. Luo, Water-assisted flash sintering: flashing ZnO at room temperature to achieve ~ 98% density in seconds, Scr. Mater. 142 (2018) 79–82.
[33] S. Funahashi, J. Guo, H. Guo, K. Wang, A.L. Baker, K. Shiratsuyu, C.A. Randall, Demonstration of the cold sintering process study for the densification and grain growth of ZnO ceramics, J. Am. Ceram. Soc. 100 (2017) 546–553.
[34] A. Ndayishimiye, K. Tsuji, K. Wang, S.H. Bang, C.A. Randall, Sintering mechanisms and dielectric properties of cold sintered (1-x)SiO_2-xPTFE composites, J. Eur. Ceram. Soc. 39 (2019) 4743–4751.
[35] X. Zhao, J. Guo, K. Wang, T. Herisson De Beauvoir, B. Li, C.A. Randall, Introducing a ZnO-PTFE (Polymer) nanocomposite varistor via the cold sintering process, Adv. Eng. Mater. 20 (2018) 1700902.
[36] T. Sada, K. Tsuji, A. Ndayishimiye, Z.m. Fan, Y. Fujioka, C.A. Randall, High permittivity $BaTiO_3$ and $BaTiO_3$-polymer nanocomposites enabled by cold sintering with a new transient chemistry: $Ba(OH)_2 \bullet 8H_2O$, J. Eur. Ceram. Soc. 41 (2020) 409–417.
[37] T. Hérisson de Beauvoir, K. Tsuji, X. Zhao, J. Guo, C. Randall, Cold sintering of ZnO-PTFE: utilizing polymer phase to promote ceramic anisotropic grain growth, Acta Mater. 186 (2020) 511–516.
[38] D. Dey, R.C. Bradt, Grain growth of ZnO during liquid-phase sintering, J. Am. Ceram. Soc. 75 (2010) 9.
[39] S.C. Pillai, J.M. Kelly, R. Ramesh, D.E. McCormack, Advances in the synthesis of ZnO nanomaterials for varistor devices, J. Mater. Chem. C 1 (2013) 3268–3281.
[40] X. Wang, P. Ren, J. Wang, J. Xu, Y. Xi, Multi-phase coexistence and temperature-stable dielectric properties in $BaTiO_3$/ZnO composite ceramics, J. Eur. Ceram. Soc. 40 (2020) 1896–1901.
[41] Z. Xu, H. Bai, S. Ma, R. Chu, J. Hao, C. Chen, G. Li, Effect of a Bi–Cr–O synthetic multi-phase on the microstructure and electrical properties of ZnO-Bi_2O_3 varistor ceramics, Ceram. Int. 42 (2016) 14350–14354.
[42] D. Xu, X. Cheng, H. Yuan, J. Yang, Y. Lin, Microstructure and electrical properties of $Y(NO_3)_3 \bullet 6H_2O$-doped ZnO-Bi_2O_3-based varistor ceramics, J. Alloys Compd. 509 (2011) 9312–9317.
[43] J. Han, P.Q. Mantas, A.M.R Senos, Sintering kinetics of undoped and Mn-doped zinc oxide in the intermediate stage, J. Am. Ceram. Soc. 88 (2011) 1773–1778.
[44] W. Onreabroy, N. Sirikulrat, A.P. Brown, C. Hammond, S.J. Milne, Properties and intergranular phase analysis of a ZnO-CoO-Bi_2O_3 varistor, Solid State Ionics 177 (2006) 411–420.
[45] M. Bartkowiak, G.D. Mahan, F.A. Modine, M.A. Alim, R. Lauf, A. Mcmillan, Voronoi network model of ZnO varistors with different types of grain boundaries, J. Appl. Phys. 80 (1996) 6516–6522.
[46] M.A. Alim, Electrical characterization of engineering materials, Act. Passiv. Electron. Compon. 19 (1996) 139–169.
[47] M.A. Alim, Influence of intrinsic trapping on the performance characteristics of ZnO-Bi_2O_3 based Varistors, Act. Passiv. Electron. Compon. 17 (1994) 99–118.